JOURNAL OF SPACECRAFT AND ROCKETS
Vol. 32, No. 3, May–June 1995

Computed Drag Reduction on a Projectile Using Porous Surfaces

Jih-Lan Hsiung*
Chung-Shan Institute of Science and Technology, Taoyuan, Taiwan, Republic of China
and
Chuen-Yen Chow†
University of Colorado, Boulder, Colorado 80309-0429

Numerical techniques are used to investigate the influence of porous surfaces on reducing the drag of secant-ogive–cylinder–boattail projectile in the transonic speed regime for Mach numbers ranging from 0.9 to 1.2 and angles of attack from 0 to 4 deg. Examined separately are the effects of angle of attack, type of porosity distribution, and maximum porosity, as well as the size and location of a porous surface placed on either the cylinder or the boattail. Computed results show that drag reductions of more than 20% can be achieved with properly arranged porous surfaces.

Nomenclature

A = area
C_D = drag coefficient
C_L = lift coefficient
C_P = pressure coefficient
M = Mach number
P = pressure
P_{inner} = pressure below the porous surface
P_{outer} = pressure above the porous surface
U_∞ = freestream velocity
V_n = velocity normal to the porous surface
X_1 = starting position of porous region in Eq. (4)
X_2 = ending position of porous region in Eq. (4)
X_k = X_1 or X_2, depending on whether X is less or greater than X_S in Eq. (5)
X_S = shock position in Eq. (5)
α = angle of attack
ξ, η, ζ = transformed coordinates in the computational space
ρ = density
ρ_{outer} = density above the porous surface
ρ_∞ = freestream density
$\bar{\sigma}$ = porosity distribution function
$\bar{\sigma}_{\max}$ = maximum porosity
ϕ = circumferential angle measured from bottom of the projectile

Introduction

TOTAL-DRAG reduction is an important consideration in the design of high-performance projectiles. For a secant-ogive–cylinder–boattail (SOCBT) projectile model such as the one shown in Fig. 1, the wave drag component is the major contributor to the total drag at transonic speeds. Thus, an effective method for drag reduction would be to weaken the shock wave and its boundary-layer interaction. The use of porous surfaces as a passive method for controlling shock boundary-layer interactions was originally suggested for reducing the wave drag of transonic airfoils. When a porous surface covering a plenum cavity is placed under a shock wave, the pressure difference across the shock induces a self-bleed upstream flow through the cavity without externally supplied power. The combination of suction downstream and blowing upstream of the shock causes the original normal shock wave on the solid surface to become a weaker lambda shock-wave system on the porous surface, resulting in reduced wave drag. A list of the related references can be found in Ref. 1 and will not be repeated here.

The porous-surface method was first applied to projectiles in the transonic speed regime by Liang and Fu[1] and was found to have similar favorable effects on drag reduction. Their numerical investigation was restricted to 0-deg angle of attack for a single Mach number of 0.96, and the porosity was only applied to the boattail of the projectile. At transonic speeds, however, shock waves most likely will appear on the cylindrical part of a solid SOCBT projectile; a porous surface placed in that region may also serve the purpose of weakening the local shock wave. Moreover, a projectile generally flies at nonzero angles of attack. For a more general analysis of a porous projectile, a numerical study is presented in this paper that includes a range of transonic Mach numbers and angles of attack. Furthermore, the location of the porous surface is no longer restricted to the boattail. It will be shown that, even at 0-deg angle of attack, the total drag may be reduced by a porous surface on the cylindrical part of a projectile where the diameter is constant.

The projectile used for all computations in this paper is the SOCBT projectile described in Refs. 2 and 3, which also present measured surface pressure data. The projectile has a 3-caliber secant-ogive nose, followed by a 2-caliber cylinder and a 1-caliber 7-deg boattail, as shown in Fig. 1.

Computational Procedure

For computing the flow about the projectile at a small angle of attack in the absence of strong boundary-layer separation, the thin-layer approximation to the full Navier–Stokes equations is often used to reduce the computational effort that is required to solve the full equations. Computations are carried out on a uniformly spaced grid in a rectangular computational space, which is transformed from physical space using grid generation techniques.

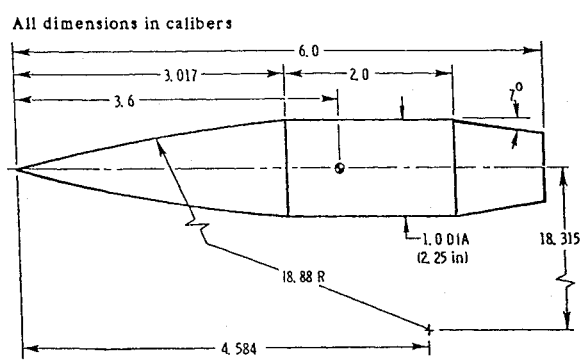

Fig. 1 SOCBT model geometry.

Received June 14, 1993; revision received Jan. 12, 1994; accepted for publication Jan. 13, 1994.

*Associate Researcher, Jet Propulsion Laboratory.
†Professor, Department of Aerospace Engineering Sciences. Associate Fellow AIAA.

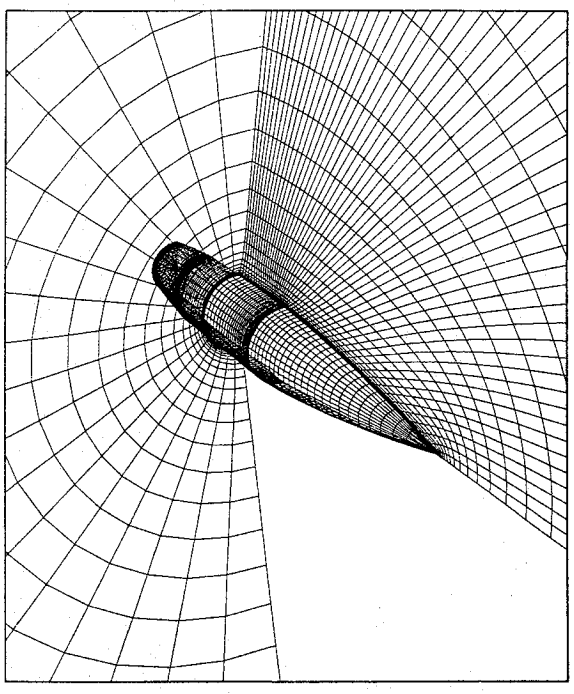

Fig. 2 Three-dimensional grid system for SOCBT model.

The numerical algorithm, grid generation scheme, initial and boundary conditions, and turbulence model are discussed separately in the following subsections, together with a brief description of various types of porous surfaces that have been adopted in this numerical study.

Numerical Algorithm

The thin-layer Navier–Stokes (TLNS) equations written in general coordinates (ξ, η, ζ) are used as the governing flow equations. Coordinates ξ and ζ are along and normal to the body in the meridional plane, respectively, and η is in the circumferential direction normal to the ξ, ζ plane. The TLNS equations are derived from the Navier–Stokes equations under the approximation that the normal gradients of the viscous stress terms are much larger than the streamwise and circumferential gradients. A description of those equations and their specific forms are given in Ref. 4. An implicit, approximately factored, flux-splitting scheme[5,6] is utilized in the computational code. Artificial dissipation operators are added to capture nonoscillatory shock profiles while maintaining computational stability. Also, a space-varying time step is used to accelerate the convergence rate.

Grid Generation

In this study, a C–O-type grid is used for the SOCBT projectile model. The grid in the meridional plane is obtained by Sorenson's elliptic solver,[7] which generates a two-dimensional finite-difference grid by solving Poisson's equation. The computational outer flowfield boundary is composed of a hemisphere whose radius is equal to 25 calibers. The computational grid has 121 points in the streamwise direction and 50 points in the direction normal to the projectile surface. This grid system is clustered near the body surface and stretched in the far field. Mesh lines nearly orthogonal to the body surface are clustered near the ogive–cylinder junction, cylinder–boattail junction, and boattail–base corner, where large gradients of flow properties are expected. The third dimension is generated by rotating the two-dimensional grid about the cylinder axis at 10-deg increments. A three-dimensional grid system is shown in Fig. 2. For a given radius, two additional grid points are needed at the circumferential boundaries to satisfy the symmetry condition there, with one at the windward ray and the other at the leeward ray, resulting in 21 circumferential points on the half body.

Initial and Boundary Conditions

For a solid SOCBT projectile, 1000 to 2000 iterations were required to reach a steady-state solution while using the freestream condition everywhere to initiate the computation. The solid-surface solution was then used as the initial condition for computing the steady-state solution for the porous projectile, which required an additional 400 to 500 iterations. On the $121 \times 21 \times 50$ grid system, with 6 s of CPU time for each iteration, a converged porous-surface solution usually took 2.5 to 4.0 CPU hours on a Cray Y-MP supercomputer.

The boundary conditions on the body are defined as follows: no-slip condition on the solid body surface, transpiration conditions on the porous surfaces, and a symmetry condition that $\partial/\partial\phi = 0$ for the circumferential boundaries of the body at $\phi = 0$ and 180 deg respectively. The pressure gradient at the projectile surface is computed from $\partial P/\partial\zeta = 0$, since the ζ coordinate is nearly orthogonal to the surface. At the far field, freestream conditions are assigned at an inflow boundary. At an outflow boundary, where constant freestream pressure is assumed, flow properties are computed using an upwind extrapolation.

Turbulence Model

The Baldwin–Lomax turbulence model[8] is used in the TLNS procedure, and was modified to include the effects of pressure gradient and normal blowing (or suction) in the boundary layer. A detailed description of the modification is given in Ref. 9.

Interface of Outer and Inner Flows

The transpiration velocity V_n from a porous surface is assumed to be governed by Darcy's law:

$$V_n = -\frac{\bar{\sigma}}{\rho_\infty U_\infty}(P_{\text{outer}} - P_{\text{inner}}) \tag{1}$$

The porosity distribution function $\bar{\sigma}$ is determined by the viscosity as well as by the size and density of the holes in the porous surface. Chen et al.[10] calculated the cavity-flow properties for transonic porous airfoils by assuming a constant total pressure in the cavity, and found that the velocity in the cavity is very low (Mach numbers less than 0.075) and that the static pressure in the cavity is almost constant. Accordingly, in the present study, a constant static pressure, $\bar{P}_{\text{inner}}$, is assumed in the cavity. For passive flow through the cavity, the requirement that the net mass flow through the porous surface of area A must be zero leads to the relation

$$\bar{P}_{\text{inner}} = \frac{\int_A \bar{\sigma}(\rho P)_{\text{outer}}\,\mathrm{d}A}{\int_A \bar{\sigma}\rho_{\text{outer}}\,\mathrm{d}A} \tag{2}$$

Once $\bar{P}_{\text{inner}}$ is known, V_n for the outer flow can be determined from Eq. (1). At nonzero angle of attack, the windward and leeward flows are different, so that the pressure in the cavity will be affected by both the porous surface and cavity structure. In this study, the efficiency of the porous surface is investigated by considering two different cavity structures. In the first cavity model, the ring-shaped cavity is divided by splitters placed at 10-deg intervals along the circumferential direction (Fig. 3). The second cavity model treats the whole cavity as interconnected. When cavities are placed on both the cylinder and the boattail, they are separate cavities that cannot communicate with each other.

Porosity Distributions

The following three types of porosity distribution have been examined, which are obtained by varying the porosity distribution function $\bar{\sigma}$ in Eq. (1):

Type 1:

$$\bar{\sigma} = \text{constant} = \bar{\sigma}_{\max} \tag{3}$$

Type 2:

$$\bar{\sigma} = \bar{\sigma}_{\max}\sqrt{\sin\frac{X - X_1}{X_2 - X_1}\pi} \tag{4}$$

Type 3:

$$\bar{\sigma} = \bar{\sigma}_{\max}\sqrt{\cos\frac{X - X_s}{X_k - X_s}\frac{\pi}{2}} \tag{5}$$

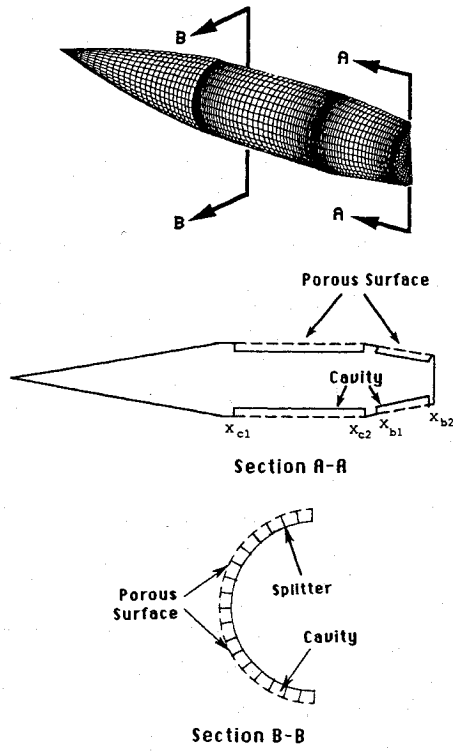

Fig. 3 Porous surface and cavity on projectile.

Type 1 porosity represents a uniform distribution throughout the entire porous region, on which V_n is determined by the pressure difference only. The type 2 porosity distribution starts from a maximum at the midpoint of the porous region and diminishes to zero toward the end points, causing higher transpiration velocities near the midpoint. The type 3 distribution automatically adjusts the porosity so that it decreases from the maximum value under the shock to zero at either end of the porous region.

Results and Discussion

All computations were for the projectile shown in Fig. 1 at a stagnation temperature of 580°R and a Reynolds number of 4.5×10^6 based on the model length. Computed cases cover Mach numbers 0.90, 0.94, 0.96, 0.98, 1.10, and 1.20 for 0-deg angle of attack, and angle of attack of 2 and 4 deg for a Mach number of 0.96.

Solid Projectile for Code Validation

The flow solver was validated using measured surface pressure data on the solid SOCBT projectile described in Refs. 2 and 3. Excellent agreement was found between computed surface pressure distributions and experimental data over a range of transonic Mach numbers and angles of attack.[11,12] Both shock strength and location were accurately determined, and the computed pressure and base drags have also been validated. The results have demonstrated the capability of the present code for computing transonic flowfields about nonporous projectiles.

Porous Projectile

A series of numerical studies was made to examine the influence of a porous surface on drag reduction on the SOCBT at Mach numbers from 0.90 to 1.20 and angles of attack of 0, 2, and 4 deg. The effectiveness of this passive control method was examined as influenced separately by Mach number, angle of attack, splitters, porosity type, maximum porosity, and the size and location of the porous region. In addition to the brief discussion presented here, a more detailed description of the computed results can be found in Refs. 11 and 12.

Effect of Mach Number at Zero Angle of Attack

The effect of porous surfaces on the SOCBT at 0-deg angle of attack is examined by applying type 1 porosity with maximum

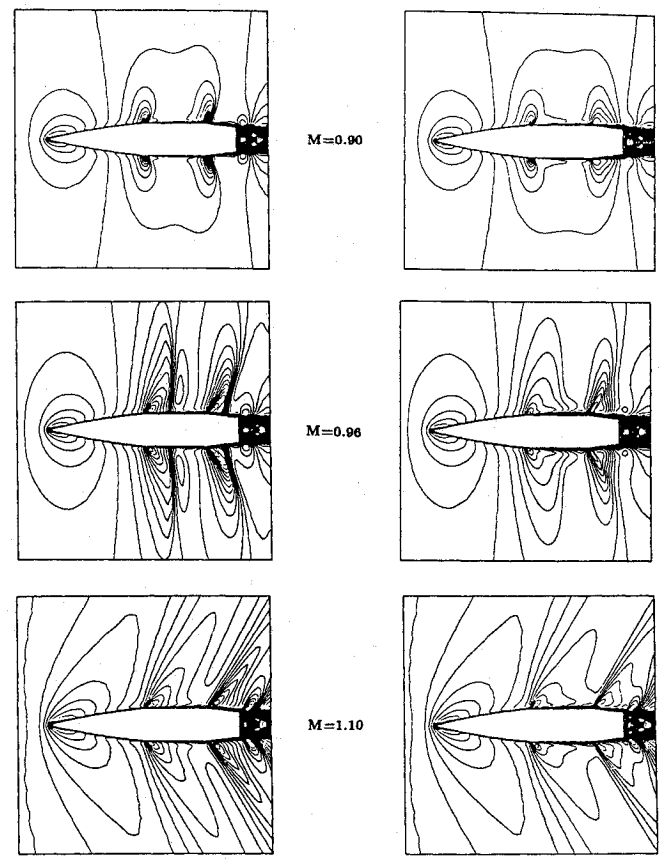

Fig. 4 Comparison of Mach contours at $\alpha = 0$ deg for type 1 porosity, $\bar{\sigma}_{max} = 0.6$.

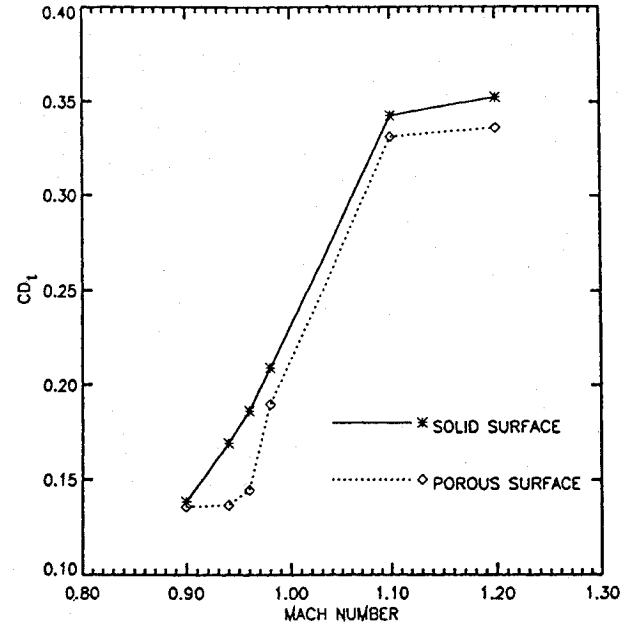

Fig. 5 Comparison of total drag coefficient of solid and porous body for type 1 porosity at $\alpha = 0$ deg.

porosity factor $\bar{\sigma}_{max} = 0.6$ on both cylinder ($3.12 \leq X_c \leq 4.99$) and boattail ($5.05 \leq X_b \leq 5.97$). The Mach-number contours for solid and porous SOCBT projectiles at Mach numbers 0.90, 0.96, and 1.10 are plotted in Fig. 4. It is clearly shown that the shock waves on the cylinder and boattail are both weakened by the porous surface. An examination of the computed subsonic flowfields reveals generally that normal suction and blowing are induced across the porous surface in the rear and front parts, respectively, and that the original normal shock waves on the solid surface are modified to become weaker lambda shocks. Figure 5 describes the effect on the

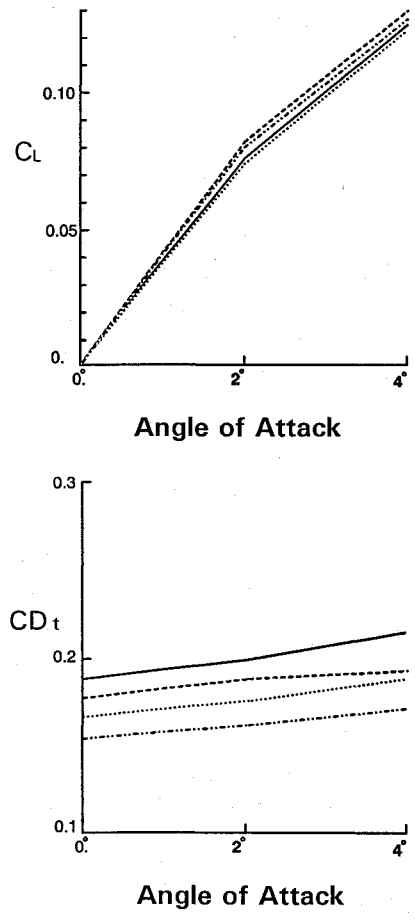

Fig. 6 Effect of porosity location on lift and drag coefficients for M = 0.96, type 2 porosity with $\bar{\sigma}_{max}$ = 0.6: M = 0.96. ———, solid; - - - - - -, boattail only; ....., cylinder only; ——.——.——, cylinder + boattail.

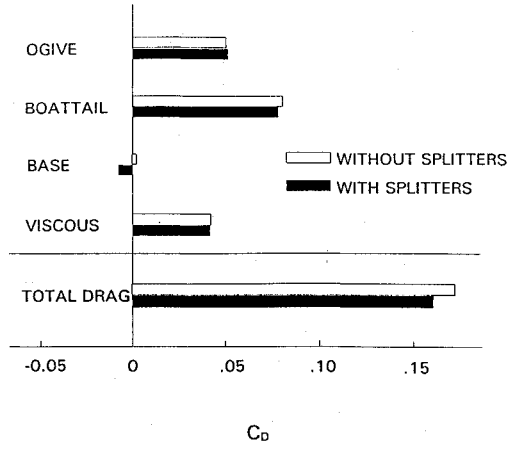

Fig. 7 Effect of splitters on drag coefficient for M = 0.96, α = 4 deg, type 1 porosity with $\bar{\sigma}_{max}$ = 0.6.

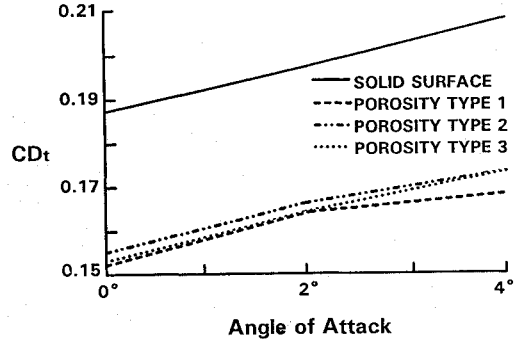

Fig. 8 Variation of total drag coefficient with angle of attack for different porosity types on both cylinder and afterbody. Here $\bar{\sigma}_{max}$ = 0.46 for type 1 porosity and 0.6 for type 2 or 3 porosity; M = 0.96.

total drag at 0-deg angle of attack of using porous surfaces on both cylinder and boattail. The porous device works particularly well at Mach numbers 0.94 to 0.98 in the presence of strong shock waves on the projectile. With this arrangement, a total drag reduction of 22.35% is achieved at $M = 0.96$.

Effects of Angle of Attack and Splitters

Figure 6 describes the effect of angle of attack on lift coefficient and total drag coefficient of the SOCBT, at Mach 0.96 and angles of attack of 2 and 4 deg, by placing a type 2 porous surface on either the cylinder or the boattail alone, or on both. For any given configuration, both C_L and C_{Dt} increase with angle of attack. A porous surface on the boattail causes the lift to increase, whereas on the cylinder it does the opposite. Generally, porosity on both the cylinder and boattail is recommended for large drag reductions.

Splitters placed in the ring-shaped cavity as shown in Fig. 2 block the communication between neighboring compartments so that the cavity pressure will vary on the circumference at nonzero angle of attack. Without splitters the cavity pressure will settle at a constant value when steady state is reached.

The effect of using splitters in the cavity is shown in Fig. 7 for Mach number 0.96 at 4-deg angle of attack. A type 1 porosity with $\bar{\sigma}_{max} = 0.6$ is used on both cylinder and boattail. To see the individual drag contributions, the total drag of the projectile is broken down into four parts, namely, the pressure drags on the ogive, boattail, and base, and the overall skin-friction drag. These components are presented in that order in Fig. 7. Data in Fig. 7 reveal that the main contribution to the reduction of total drag by splitters is from the sign reversal of the base drag.

Effect of Porosity Type

To investigate the effect of varying the type of porosity on drag reduction, porosity distributions of types 1–3, defined in Eqs. (3–5), are presented. Porous surfaces of the same type are used on both the cylinder and boattail at a Mach number of 0.96. For a fair comparison, the total porosity of a porous surface, defined as the integral of $\bar{\sigma}\,dx$ over that surface, must be kept the same when the porosity type is changed. The value of $\bar{\sigma}_{max}$ adopted for the present numerical computation is 0.46 for type 1 porosity and 0.6 for either type 2 or 3. The computed C_p distributions for different types of porosity at 0-deg angle of attack reveal that type 1 porosity is more effective in weakening the shock strength than types 2 and 3, since it provides a stronger blowing at the beginning of the porous region. The effects of types 2 and 3 are comparable, because the shock waves in both cases are located near the center of the local porous region. Type 1 porosity gives a base pressure that is higher than that from either type 2 or type 3 porosity, because of the stronger suction at the rear end of the type 1 porous region on the boattail.

Compared in Fig. 8 are the variations of the total drag coefficient with angle of attack of different porosity types. It appears that the type 1 porosity is more effective for drag reduction in the present arrangement.

Effect of Maximum Porosity

The effect of varying the maximum porosity on the performance of a porous projectile has been examined by using four different values of $\bar{\sigma}_{max}$, namely 0.1, 0.3, 0.6, and 0.8, at a Mach number of 0.96 and at angles of attack of 0, 2, and 4 deg. Porous surfaces of type 1 are located from $X = 3.03$ to 4.99 on the cylinder, and from $X = 5.05$ to 5.97 on the boattail. In general, the computed result indicates that a larger value of $\bar{\sigma}_{max}$ has a greater effect on reducing the shock strength, but as $\bar{\sigma}_{max}$ continuously increases its effectiveness will approach a limit. Furthermore, a larger value of $\bar{\sigma}_{max}$ causes a higher base pressure, resulting in a smaller base drag.

Variations of C_{Dt} with $\bar{\sigma}_{max}$ at different angle of attack are plotted in Fig. 9. This figure reveals the general trend the total drag

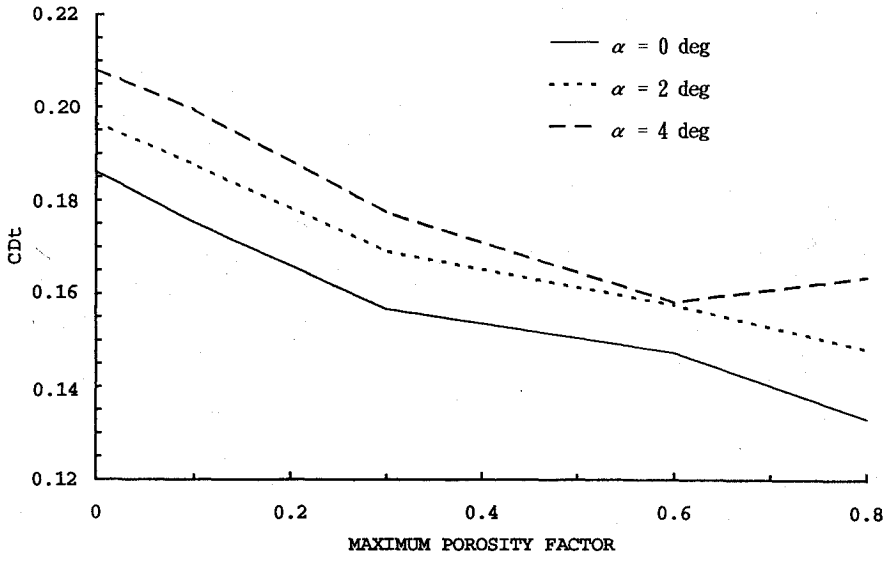

Fig. 9 Variation of total drag coefficient with angle of attack for different $\bar{\sigma}_{max}$ for type 1 porosity at $M = 0.96$.

Table 1 Effect of porous surface size and location of drag components, for type 2 porosity, $\bar{\sigma}_{max} = 0.6$, $M = 0.96$, and $\alpha = 0$ deg

Model[a]	Porous position	C_D Ogive	Boattail	Base	Viscous	Total	Total-drag reduction,%
A	None	0.0311	0.0972	0.0033	0.0545	0.1861	Reference
B	3.03–4.99	0.0302	0.0754	0.0061	0.0539	0.1656	11.02
	3.03–4.51	0.0306	0.0868	0.0045	0.0462	0.1682	9.62
	3.48–4.99	0.0307	0.0910	0.0046	0.0589	0.1852	0.48
	3.03–4.02[b]	0.0304	0.0879	0.0050	0.0453	0.1686	9.40
	3.25–4.26[b]	0.0307	0.0898	0.0052	0.0453	0.1710	8.11
	3.48–4.51[b]	0.0308	0.0944	0.0041	0.0524	0.1817	2.36
	3.78–4.76[b]	0.0308	0.0917	0.0049	0.0560	0.1835	1.40
C	5.05–5.97	0.0311	0.0951	−0.0004	0.0487	0.1745	6.23
	5.05–5.75	0.0308	0.0950	0.0033	0.0502	0.1793	3.66
	5.26–5.97	0.0308	0.0966	0.0006	0.0514	0.1794	3.60
	5.26–5.75	0.0308	0.0904	0.0064	0.0501	0.1776	4.57

[a]Model A: solid surface; B: porous surface on cylinder only; C: porous surface on boattail only.
[b]Porous length ≈ 1.0.

decreases as $\bar{\sigma}_{max}$ increases except for the $\alpha = 4$-deg curve, which shows that C_{Dt} increases as $\bar{\sigma}_{max}$ increases from 0.6 to 0.8. In other words, increasing $\bar{\sigma}_{max}$ beyond 0.6 may not further improve the performance at 4-deg angle of attack. A total drag reduction as high as 28.43% is found for Mach number 0.96 at 0-deg angle of attack with $\bar{\sigma}_{max} = 0.8$.

Effect of the Size and Location of the Porous Region

The effect of varying the length and location of a porous region is investigated separately for the porous surface on the cylinder and on the boattail of a SOCBT at 0-deg angle of attack. The results obtained for a type 2 porosity with $\bar{\sigma}_{max} = 0.6$ are summarized in Table 1. For the case of a porous surface on the cylinder, a maximum total drag reduction of 11.02% is achieved by the longest porous region. For a porous surface of length of about 1.5, the forward position provides a much larger drag reduction than the rearward position. The same behavior has also been found for a porous surface of shorter length.

On the other hand, for a porous surface on the boattail of a fixed length, varying its position does not cause a significant change in total drag reduction. But a longer porous region still gives a larger drag reduction, as represented by the case for the longest porous region.

The total-drag reduction is directly related to both the size and location of the porous region on the cylinder. According to the computation, a longer porous surface gives a better performance than a shorter one. As far as the location is concerned, it seems to be more efficient to reduce the total drag by placing the porous surface at such a position that its rear part is under the original shock wave on the solid projectile.

Conclusions

Transonic flows over a SOCBT projectile at angle of attack up to 4 deg have been simulated by solving the TLNS equations numerically with a modified Baldwin–Lomax turbulence model and a porosity model governed by Darcy's law. The code was validated by comparison with the experimental pressure data. The code has been employed to investigate the effects of porous surfaces as passive devices for reducing the total drag on a projectile at transonic speeds.

Computations show that placing porous surfaces on both cylinder and boattail at transonic Mach numbers can change the original normal shock waves to weaker lambda shock systems. The porous surface is more effective at drag reduction at Mach numbers 0.94 to 0.98 in the presence of strong shock waves on the projectile. With a nonzero angle of attack, lift can be increased with an appropriate porosity distribution, and the drag reduction efficiency can be improved if splitters are put in the cavity under the porous surface.

Parameters pertaining to a porous surface, such as the distribution type, maximum porosity, and size and location, have been investigated to evaluate their influences on drag reduction. The results show that the total drag can be decreased by placing a porous surface on either the cylinder or the boattail section of the projectile. For the present model type 1 porosity distribution provides better performance than types 2 and 3, and type 3 is superior to type 2 at $\alpha < 4$ deg for drag reduction. The drag reduction efficiency increases with maximum porosity for type 1 porosity, and a limiting value of 0.6 has been found for the maximum porosity factor at Mach number 0.96 and 4-deg angle of attack, above which the efficiency will start to diminish. The porous surface is more efficient if the normal shock on the solid surface is in the rear part of the porous region. On the other hand, drag reduction efficiency improves with increasing size of the porous surface.

Acknowledgment

The authors would like to thank Cray Research, Inc., for granting supercomputer time on the Cray Y-MP at the University Corporation for Atmospheric Research.

References

[1]Liang, S. M., and Fu, J. K., "Passive Control Method for Drag Reduction of Transonic Projectiles," AIAA Paper 91-3213, Jan. 1991.

[2]Kayser, L. D., and Whiton, F., "Surface Pressure Measurement on a Boattailed Projectile Shape at Transonic Speeds," U.S. Army Ballistic Research Lab., Rept. ARBRL-MR-03161, Aberdeen Proving Ground, MD, March 1982.

[3]Kayser, L. D., "Base Pressure Measurements on a Projectile Shape at Mach Numbers from 0.91 to 1.20," U.S. Army Ballistic Research Lab., Rept. ARBRL-MR-03353, Aberdeen Proving Ground, MD, April 1984.

[4]Hoffmann, K. A., *Computational Fluid Dynamics for Engineers*, 1st ed., Engineering Education System, Austin, TX, 1989, pp. 476–478.

[5]Ying, S. X., Steger, J. L., Schiff, L. B., and Baganoff, D., "Numerical Simulation of Unsteady, Viscous, High-Angle-Attack Flows Using a Partially Flux-Split Algorithm," AIAA Paper 86-2179, Aug. 1986.

[6]Ying, S. X., "Three-Dimensional Implicit Approximately Factored Schemes for Equations in Gasdynamics," Ph.D. Thesis, Stanford Univ., Stanford, CA, June 1986.

[7]Sorenson, R. L., "A Computer Program to Generate Two-Dimensional Grid about Airfoils and Other Shapes by the Use of Poisson's Equation," NASA-TM-81198, 1980.

[8]Baldwin, B. S., and Lomax, H., "Thin Layer Approximation and Algebraic Model for Separated Turbulent Flows," AIAA Paper 78-257, Jan. 1978.

[9]Crawford, M. E., and Kays, W. M., "STAN5—A Program for Numerical Computation of Two-Dimensional Internal and External Boundary Layer Flows," NASA-CR-2742, Dec. 1976.

[10]Chen, C.-L., Chow, C.-Y., Van Dalsem, W. R., and Holst, T. L., "Computation of Viscous Transonic Flow over Porous Airfoils," *Journal of Aircraft*, Vol. 26, No. 12, 1989, pp. 1067–1075.

[11]Hsiung, J.-L., "Computation of Transonic Flow over a Porous Surface Projectile," Ph.D. Thesis, Univ. of Colorado, Boulder, CO, April 1992.

[12]Hsiung, J.-L., and Chow, C.-Y., "Drag Reduction of Transonic Projectile by Porous Surface," AIAA Paper 93-0417, Jan. 1993.

J. M. Allen
Associate Editor